Received: 8 April 2024 | Revised: 12 August 2024 | Accepted: 19 August 2024

DOI: 10.1111/joa.14133

Journal of Anatomy ANATOMICAL SOCIETY WILEY

ORIGINAL ARTICLE

Multiple exostoses and an osteochondroma in a Pliocene canid from Langebaanweg 'E' Quarry (South Africa)

Anusuya Chinsamy[1] | Alberto Valenciano[2,3]

[1]Department of Biological Sciences, University of Cape Town, Cape Town, South Africa

[2]Departamento de Geodinámica, Estratigrafía y Paleontología, Facultad de Ciencias Geológicas, Universidad Complutense de Madrid, Madrid, Spain

[3]Research and Exhibition, Iziko Museums, Cape Town, South Africa

Correspondence
Anusuya Chinsamy, Department of Biological Sciences, University of Cape Town, Private Bag X3, Rhodes Gift, 7701 Cape Town, South Africa.
Email: anusuya.chinsamy-turan@uct.ac.za

Alberto Valenciano, Departamento de Geodinámica, Estratigrafía y Paleontología, Facultad de Ciencias Geológicas, Universidad Complutense de Madrid, C/José Antonio Novais 12, Madrid 28040, Spain.
Email: albvalen@ucm.es

Funding information
MCIU/AEI/10.13039/501100011033/FEDER, UE, Grant/Award Number: PID2023-151089NB-I00; National Research Foundation, Grant/Award Number: 136510; Research Group UCM, Grant/Award Number: 910607; Ministerio de Investigación e Innovación, Grant/Award Number: PID2020-116220GB-I00

Abstract

Langebaanweg is a Mio-Pliocene locality located on the West Coast of South Africa. It is renowned for its rich diversity of both terrestrial and marine vertebrate fossils. Several carnivorans have been identified from this site, amongst which is the recently described jackal-like canid, *Eucyon khoikhoi*. One of the skeletons assigned to *E. khoikhoi* exhibits anatomical deformities on several bones of the skeleton. Here, we use multiple methodologies (anatomical descriptions, CT scanning and histology) to investigate the bony overgrowths or exostoses evident in the radius, and we compare these findings with those of a radius from a healthy individual of the same species from Langebaanweg. Our results show that anatomical observations are important for first level observation of the pathology, but that micro-CT scanning permits a more precise assessment of how the pathology affected the internal organization of the bone, both periosteally and endosteally. This methodology permitted us to diagnose the tumors as benign rather than cancerous. Our observations of calcified cartilage in the histological thin sections in the region of the exostosis allowed us to further diagnose the exostosis as an osteochondroma. This study has demonstrated the usefulness of applying multiple techniques to characterize and diagnose pathological bony growths in a fossil canivoran. We have also demonstrated the usefulness of histological studies in permitting a more refined diagnosis of the exostosis as an osteochondroma.

KEYWORDS
carnivora, neogene, osteopathology, palaeopathology

1 | INTRODUCTION

The Mio-Pliocene locality of Langebaanweg (situated within the West Coast Fossil Park) on the Southwestern coast of the Western Cape Province of South Africa is globally known for its rich vertebrate fossils that are dated to ~5.2 million years ago (Roberts et al., 2011). Since the discovery of fossils at this locality more than 60 years ago, there have been a host of studies that have documented the diversity of terrestrial and marine animals that existed here during the early stage of the Early Pliocene transgression (e.g., Bernor & Kaiser, 2006; Gentry, 1980; Govender et al., 2012; Harris, 1976; Hendey, 1970, 1973, 1982; Hendey & Gentry, 1970; Jiangzuo et al., 2023; Matthews et al., 2007; Valenciano et al., 2022; Valenciano & Govender, 2020a, 2020b).

Initially, Brett Hendey recognized a number of the Langebaanweg carnivorans (Hendey, 1974, 1978a, 1978b, 1980, 1981, 1982), and

over the next few decades there have been various other reports (e.g., Govender, 2015; Hunt Jr, 1996; Werdelin, 2006; Werdelin et al., 1994). More recently, Valenciano et al. (2022) described *Eucyon khoikhoi*, a new species of a jackal-like canid from the Langebaanweg 'E' Quarry. This medium-sized canid, with an estimated weight of about 9 kg, suggests a direct relationship with the extant *Schaeffia adusta* (side-striped jackal) and confirms the presence of this group in Africa more than 5 million years ago. Like *S. adusta*, *E. khoikhoi* is interpreted as an omnivorous scavenger. In the taxonomic diagnosis of *E. khoikhoi*, Valenciano et al. (2022) mentioned that another specimen also ascribed to *E. khoikhoi* SAM-PQL40041 exhibited several skeletal anomalies that were probably pathological: overgrowths of bone were noted on the periosteal surfaces of the long bones, metacarpals, phalanges and a caudal vertebra, and endosteal bony growths were observed around the medullary cavity of a broken metacarpal IV and a radius. Although Hendey (1974, 1982) had noted deformities in the skeletal remains of several Langebaanweg vertebrates, there have only been a few studies that have attempted to assess the nature of the pathologies in these taxa: sivatheres (Franz-Odendaal et al., 2004); seals (Govender et al., 2011; Woolley et al., 2019), and a sabretooth cat (Rabe et al., 2022).

Studies of pathologies in extinct animals provide fascinating insight into diseases that affected prehistoric animals (e.g., Anné et al., 2015; Chinsamy & Tumarkin-Deratzian, 2009; de Souza Barbosa et al., 2013; Ekhtiari et al., 2020; Fernández-Monescillo et al., 2019; González et al., 2017; Haridy et al., 2019; Heckert et al., 2021; Iurino et al., 2015; Lucas & Schoch, 1987; Moncunill-Solé et al., 2019; Moodie, 1923; Rabe et al., 2022) and in some cases permit deductions regarding how the particular trauma may have affected the behavior of the animal (e.g., Iurino et al., 2013; Rabe et al., 2022; Redelstorff et al., 2015). Several studies have described pathologies in extinct carnivores (e.g., Domingo et al., 2012; Iurino et al., 2013, 2015; Iurino & Sardella, 2015; Luna et al., 2023; Slabá et al., 2018; Wang et al., 2023), and some have specifically focused on canids (e.g., Bartolini-Lucenti et al., 2021; Rothschild et al., 2001; Tong et al., 2020; Wang & Rothschild, 1992; Werdelin & Lewis, 2013), although it is evident that the majority of these studies have focused on dental or oral pathologies. Furthermore, most of these studies combined anatomical descriptions with computer tomography (CT) scanning but rarely has the osteohistology of the pathology been investigated (e.g., Woolley et al., 2019).

By investigating the internal microstructural organization of the bone (i.e., its microstructure or osteohistology) more insight can be obtained to characterize the pathological tissues (Anné et al., 2015). For instance, while CT scanning provides a non-destructive 3D view of the internal organization of the bone, osteohistological studies allow the identification of the tissues that form the pathology. Thus, a combination of these different methodologies affords greater insight into the nature of the palaeopathology.

Interestingly, even though there has been an increasing number of studies on the osteohistology of extinct mammals (e.g., Hill, 2006; Jannello & Chinsamy, 2023; Kolb et al., 2015; Nacarino-Meneses et al., 2016; Nacarino-Meneses & Chinsamy, 2022; Seymour et al., 2018), as well as on extant mammals (e.g., Calderón et al., 2021; Chinsamy & Warburton, 2021; Kohler & Moya-Sola, 2009; Kolb et al., 2015; Legendre & Botha-Brink, 2018; Montoya-Sanhueza et al., 2021; Montoya-Sanhueza & Chinsamy, 2018), most of these studies have focused on bones that were recovered from non-diseased individuals. However, there are a few palaeohistological studies that have identified and described pathological bone tissues in extinct mammals, for example, seals (Woolley et al., 2019). Except for the latter study, which included anatomical descriptions, and micro-CT scanning, as well as osteohistological assessment of the phocid seals from Langebaanweg, all the previous investigations on the pathologies that affected the Langebaanweg vertebrates were based on gross anatomical observations.

In the current study, we utilize multiple methods (i.e., gross macro-anatomical descriptions, micro-anatomical observations [through micro-CT scanning], and osteohistology) to characterize and diagnose the nature of the pathologies that afflicted the skeleton (and more specifically the radius) of the Langebaanweg jackal-like canid, *E. khoikhoi*.

2 | MATERIALS AND METHODS

As mentioned previously in the original description of *E. khoikhoi*, it was recognized that the skeleton of specimen number SAM-PQL40041 showed several pathological features (Valenciano et al., 2022). Since histological sectioning is destructive, the South African Heritage Agency (SAHRA permit number: 13721) permitted us to section just the radius of the disease-ridden skeleton of *E. khoikhoi* (SAM-PQL40041), and an equivalent bone from a healthy specimen of *E. khoikhoi* (SAM-PQL31272). Both radii were fragmented, minimizing the degree of destruction of the bones, and thereby averting the cutting of complete bones. Both specimens (Figures 1 and 2) were recovered from the Pliocene Langebaanweg 'E' Quarry (LBW) locality on the West Coast of South Africa and the material is currently housed in the Cenozoic collections of Iziko Museums of South Africa in Cape Town.

The radius of both specimens was micro-CT scanned at the University of Stellenbosch Scanning Facility (du Plessis et al., 2016) in the Western Cape Province of South Africa. Using the guidelines outlined by du Plessis et al. (2017), the General Electric V|TomeX L240 system was used to scan the bones. Each specimen was scanned using the following specifications: 80 kV (voltage), 240 μA (current), and 100μ resolution. Visualization and analysis of the micro-CT scanned data were obtained using Volume Graphics (MyVGL). Images were imported into Coreldraw and prepared for publication.

Both shafts of the radii were prepared for histological analyses using standard methods for processing undecalcified fossil bone (Chinsamy & Raath, 1992) in the Department of Biological Sciences at the University of Cape Town. Figure 2 indicates where the bones were sectioned, and Table 1 indicates the slides that were prepared from each of the radii. The samples were embedded in clear resin

FIGURE 1 Selected mandibular and postcranial remains of *Eucyon khoikhoi* SAM-PQL40041 from Langebaanweg 'E' Quarry showing the pathological bones. (a, b) Right hemimandible in buccal (a) and lingual (b) views. (c, d) Right fragmentary humeral head in caudal (c) and medial (d) views. (e, f) Right fragmentary ulna in medial (e) and caudal (f) views. (g, j) Left fragmentary radius in cranial (g), lateral (h), caudal (i) and medial (j) views. (k) Right mounted manus in dorsal view composed by the Metacarpal II-V, and several first, second, and ungual phalanges from uncertain anatomical element (both manus or pes). (l, m) Fourth caudal vertebra in dorsal (l) and ventral (m) views. (n) Left pyramidal in lateral view. (o) Left magnum in medial view. (p) Right ectocuneiform in lateral view. (q–s) First phalange in dorsal (q), lateral (r) and proximal (s) views. (t) First phalange in dorsal view. (u–x) Second phalange in dorsal (u), lateral (v), palmar/plantar (w), and proximal (x) views. (y, z) Ungual phalange in lateral (y) and proximal (z) views. Scale bar equals 5 cm (a–m), and 2 cm (n–z).

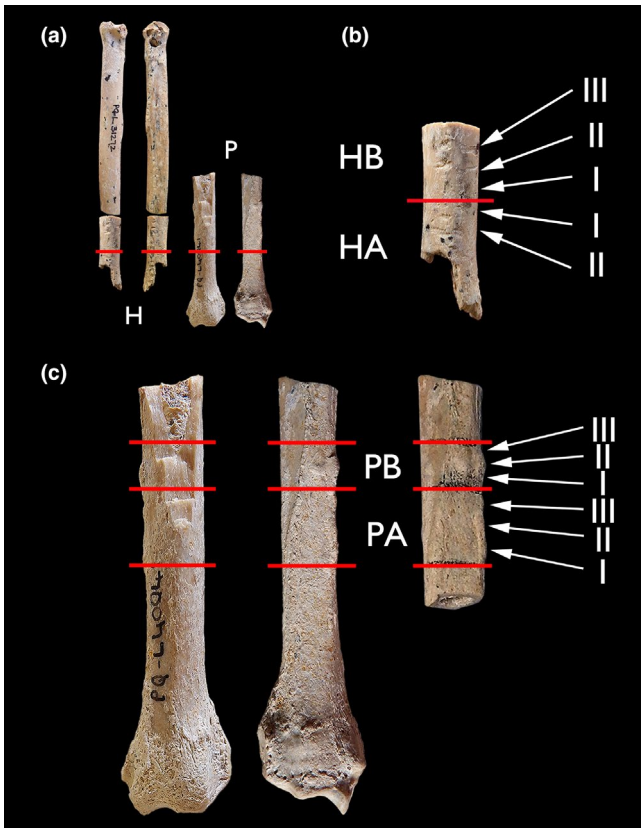

FIGURE 2 Analyzed radii of *Eucyon khoikhoi* from Langebaanweg 'E' Quarry for paleohistological analyses. (a) General view of the fragmentary radius of SAM-PQL31272 that corresponds with a healthy individual in cranial and caudal views respectively, and fragmentary radius of SAM-PQL40041 with pathologies in cranial and caudal views. (b) Specifications of the cuts performed over SAM-PQL31272. (c) Specifications of the cuts performed over SAM-PQL40041 in cranial and caudal views. Red lines specify the exact area of the cuts, white arrows indicate the position of the successive serial cuts for each fragment of the radius cut. A, B indicate sectioned blocks; H, healthy specimen; P, pathological specimen.

consisting of a mixture of Epoxacast 690 resin and Epoxacast 690 hardener in the ratio 100:30. Each radius was sectioned and labelled as indicated in Figure 2. The exposed surface of each block was polished using a series of abrasive carbide grinding discs (400p, 600p, and 1200p) on the IMP Imptech polishing machine. The final polishing was done using a velvet cloth covered lap-wheel with a solution of Struers OP-U. Once smooth and well-polished, the block was then mounted onto a frosted petrographic slide using Epoxacast resin

TABLE 1 List of the thin sections prepared from the healthy radius (H) and the pathological radius (P).

Specimen	Slides
Eucyon khoikhoi	
SAM-PQL40041, Pathological radius	PAI
	PAII
	PAIII
	PBI
	PBII
	PBIII
SAM-PQL31272, Healthy radius	HAI
	HAII
	HBI
	HBII
	HBIII

Note: Refer to Figure 2 to see the location of the thin sections on the shaft of the bone.

and Epoxacast hardener. Thin sections were cut off the mounted blocks using a precision cut-off machine (Struers Accutom), and the cut surfaces were then ground down using graded carbide grinding discs. During the grinding process, sections were checked frequently under the microscope until the optimal thickness to view the microstructure of the bone (about 50–30 μm) was reached. High quality photomicrographs were taken using normal, and polarized light using a Nikon Eclipse E200 polarizing microscope and a Zeiss AX10. NIS-Elements microscope imaging software by Nikon for producing micrographs; Kolor Autopano Giga (APG) software was used for making composite images and all images were edited using Coreldraw version 14, 2022.

3 | RESULTS

3.1 | Anatomical description

In particular, the abnormal bones in *E. khoikhoi* SAM-PQL40041 are both hemimandibles, the right proximal epiphysis of the humerus, the right proximal epiphysis of the ulna, the left distal epiphysis of the radius, the complete right metacarpals II, III and V, and a broken right Mc IV, the left both pyramidal and magnum, the right ectocuneiform, several sesamoids, four first phalanges, three second phalanges, one

ungual phalanx and the fourth caudal vertebra (Figure 1). The surface of these bones appears irregular with globular textures that form bulging areas between the ligamentous area of the carpals and the ectocuneiform, as well as in the dorsal and palmar areas of the metacarpals. In the areas close to the epiphysis of the humerus, radius, ulna, and phalanges, the bony overgrowths are more prominent and form distinct bulges. Similar overgrowths are visible in the endosteal region of the IV metacarpal and the radius. In the mandibles, the pathology appears to be different: there is a loss of the mandibular corpus around the tooth root, and the bony overgrowths form a continuous band over the roots of the lower first to the second molars and appear to be more developed in the right hemimandible. Additionally, a white-to-grey porous layer appears over the roots of the teeth.

3.2 | Micro-CT scanning results

The CT scans of the bones provided insight into the 3D structure of the normal and pathological radii. The longitudinal scans of the radii permit an assessment of the microanatomy of the bones.

3.2.1 | Normal bone, SAM-PQL31272

The normal bone appears to have an evenly thick bone wall all along the shaft of the bone that surrounds a vacant medullary cavity (Figure 3a,b). The periosteal and endosteal surface of the bone appears to be smooth without any signs of resorption or excavations into the bone wall (Figure 3a,b). In general (except for some post-mortem cracks during fossilization), the entire bone wall appears to comprise predominantly compact bone tissue, with just a few erosion cavities evident (Figure 3a,b).

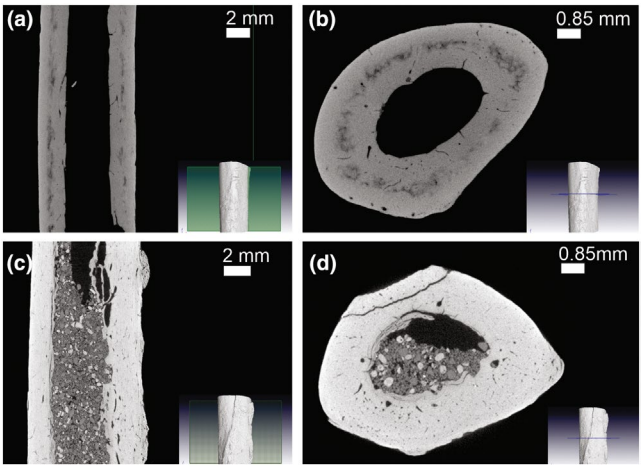

FIGURE 3 CT scan images of the healthy radius (a, b), and the pathological radius (c, d). (a) and (c) are longitudinal views of the bones, whilst (b) and (d) are cross sectional views of the microanatomy. Note that in the healthy radius, the bone wall thickness is relatively even, and both the periosteal and endosteal surfaces appear to be smooth. However, in the pathological radius, notice the uneven thickness of the medial and lateral walls of the diaphysis, and the excavated, uneven endosteal surface of the bone. On the medial side of the bone, some lumps of bony growth are visible. Note also that the pathological bone appears to have many more cavities present in the bone wall.

3.2.2 | Pathological bone, SAM-PQL40041

Although the gross anatomy allowed an assessment of the distribution of the bony growths, the CT scan permitted insight into how such deviant growth affected the entire bone wall. The medial part of the bone wall appears to have the most pronounced bony growth, but it is evident that such growths extend all along the medial aspect of the shaft (Figure 3c). The longitudinal view through the thickest part of the shaft shows how disproportionate is the thickness of the bone wall (Figure 3c): the medial side of the bone wall appears to be substantially thicker than the lateral side of the bone wall which interestingly appears thinner than the normal bone wall thickness of the unaffected radius (Figure 3a). The entire periosteal surface of the medial side of the bone appears to be overlain by the bony growths, and it is evident that the endosteal margin on the medial side of the bone is also severely affected, with some irregular bone deposits on the endosteal side of the lateral bone wall (Figure 3c,d). In the latter region, there appear to be excavations into the bone wall. Overall, the medial bone wall is much more "porous" with many more erosion cavities visible as compared to the lateral side of the bone wall. The medullary cavity is mostly vacant, although there are occasional struts that extend from the pathological medial endosteal side into the medullary cavity.

3.2.3 | Osteohistology of the normal and pathological radii

Histology of "normal" radius, SAM-PQL31272

The thin sections of this radius confirmed that the bone wall comprised of essentially compact bone (without erosion cavities) that surrounded the medullary cavity (Figure 4a). The bone is richly vascularized with vascular canals that tend to have a more reticular arrangement, and which are embedded in a woven bone matrix. The medullary cavity is lined by a distinct layer of lamellar bone tissue, the Inner Circumferential Layer (ICL), wherein the osteocyte lacunae are all flattened and tend to be elongated (Figure 4b). The thickness of the ICL is variable across the section, with the thickest part in the lateral part of the bone wall. In this anterior region, there is a small trabecula that projects into the medullary cavity (Figure 4b). Other than this, the medullary is completely free of any bony tissue. Preceding the ICL, in most of the compacta there appears to be a large amount of compacted coarse cancellous bone (cccb), which indicates that this region of the shaft was close to the metaphysis of the growing bone (Figure 4a,d). There are secondary osteons scattered throughout the compacta, but they mostly tend to be located mid-cortically with some occasional ones nearer the periosteal surface (Figure 4c). In the medial part of the bone wall, periosteally, a

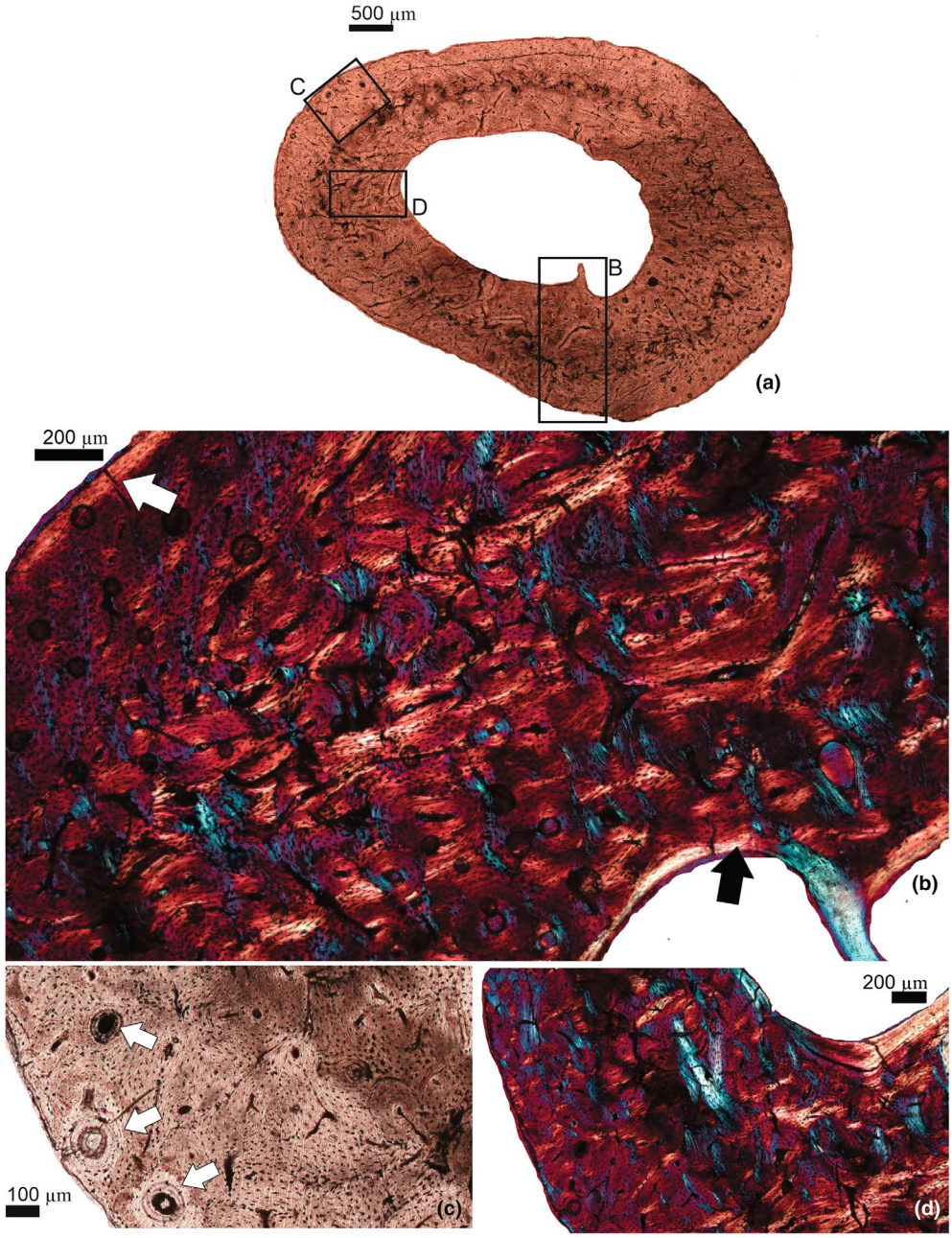

FIGURE 4 Osteohistology of the healthy radius, thin section HAI. (a) Overview of the thin section, showing the vacant medullary cavity that is surrounded by a thick layer of compacted bone. (b) Higher magnification of the framed region in (a), showing the OCL (white arrow) and the ICL (black arrow). (c) Higher magnification of the framed region in (a) showing some detail of the secondary osteons (white arrows) and primary osteons near the periosteal margin of the bone wall. (d) Higher magnification of the framed region in (a), showing compacted coarse cancellous bone tissue that makes up most of the bone wall in the endosteal region of the compacta. (b) and (d) use a ¼ lambda filter and polarized light. ICL, inner circumferential layer; OCL, outer circumferential layer.

narrow, outer circumferential layer (OCL) comprising lamellar bone tissue is visible, indicating that this bone was from a young adult (Figure 4b). This layer is thin and not uniformly distributed across the thin section, with some areas (like the posterior margin) lacking any such deposits.

Histology of the pathological radius, SAM-PQL40041

The CT scan of the pathological radius (Figures 3a–c and 5; Table 1) showed that the medial margin of the bone wall was most severely affected, although the bony growths also extended toward the posterior parts of the bone wall. The thickness of the bone wall across the section varies, with the thickest part of the bone wall in the posterior-medial region. The bony growths on the surface of the bone are more developed in the medial region (Figure 3c,d). In the posterior region, the overlaying bony growth layer is generally narrow, with just a slight bulge in the mid-posterior part of the bone wall.

The normal peripheral margin of the bone wall comprises a distinct wide OCL consisting of lamellar bone (Figure 5a–c), which

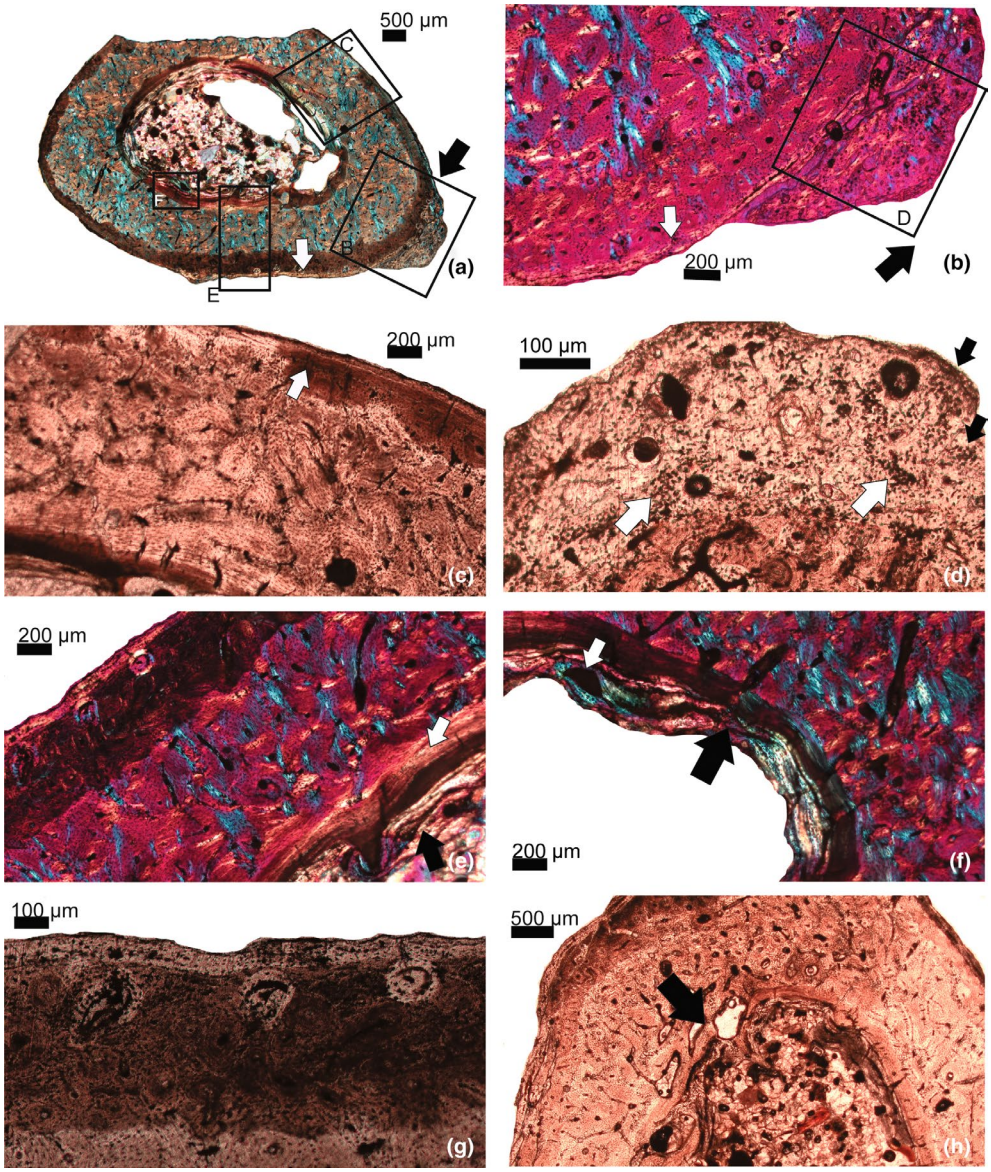

FIGURE 5 Osteohistology of the pathological radius (SAM-PQL40041). (a) Overview of the thin section PAI. Black arrow indicates the pronounced overgrowth in this region of the bone wall, White arrow indicates the poorly vascularized outer part of the compacta. (b) Higher magnification of the periosteal parts of the compacta including the bony overgrowth (black arrow). White arrow showing the poorly vascularized periosteal bone tissues of the OCL. (c) Higher magnification of the bone wall showing the poorly vascularized bone tissue in the peripheral part of the bone wall (white arrow). (d) Higher magnification of the exostosis showing the patches of calcified cartilage near the margins, some in columns (small black arrow), as well as islands of calcified cartilage (white arrows). Overall, this exostosis is richly vascularized. (e) Higher magnification of the bone wall using a lambda filter, showing fibro-lamellar bone tissue with many vascular canals in the mid-cortical region. In the endosteal region a distinct ICL (white arrow) comprising of lamellar bone tissue is visible. This tissue is overlain by a more woven type tissue (black arrow) with more globular osteocyte lacunae and vascular canals. (f) The black arrow indicates the more woven textured pathological bone that lines the medullary cavity. Note the blood vessels in this tissue, one of which is enlarged to form an erosion cavity (white arrow). (g) Higher magnification of the peripheral region in (e) showing the diagenetically altered tissue. (h) Several enlarged erosion cavities (black arrow) near the perimedullary margin extend into the ICL (a), (b), (e), (f) use a ¼ lambda filter and polarized light. (a), (c), and (e–g) are from thin section PA1, whereas (b), (d), and (h) are from thin section PAII. ICL, inner circumferential layer; OCL, outer circumferential layer.

indicates that this individual was a mature adult. Below this narrow band of tissue, the bone wall comprises predominantly of fibro-lamellar bone with many vascular canals, several of which are enlarged due to resorption (Figure 5c,d,h). Several secondary osteons occur right up to the original periosteal margin of the bone wall (Figure 5e,g). Some of the peripheral bone tissue (including the secondary osteons) near the region of the bony growth appears to be diagenetically altered (Figure 5g). The endosteal margin consists of an ICL, which comprises of a thick layer of lamellar bone, that is overlain by a layer of woven bone tissue with vascular

canals, some of which show secondary resorption (Figure 5e,f). In some areas, remnants of the swirled lamellar texture of cccb are visible (see Figure 5a,c), which indicates that during early ontogeny this part of the bone wall was in the metaphysis. In the medio-anterior region, there are large erosion cavities visible in the ICL, and trabecular bone extends into the medullary cavity (Figure 5a,f,h). It should also be noted that the endosteal margin appears to be quite resorptive with excavations that extend into the underlying bone tissue (Figure 5h). In anterior-lateral side of the bone wall, there appears to be deposits of unusual endosteal bone tissue that appears to be more woven textured with dense number of globular osteocyte lacunae, and a few erosion cavities (Figure 5e,f). In the medial part of the bone wall, erosion cavities are visible (Figure 5h). Several Volkmann's canals extend from the medullary cavity into the ICL (Figure 5c,h).

The largest of the bony outgrowths is on the medial side of the bone wall. The bone comprises of a woven textured bone matrix, in which many globular osteocyte lacunae are located, although islands of calcified cartilage are also evident in this mass of bone tissue (Figure 5b,d). Several enlarged erosion cavities are also visible in this bony outgrowth (Figure 5d). The surface of this bone appears crenulated, and along the margin of the outgrowth, some calcified cartilage is visible. Some of these are clearly aligned one below the other -like tracts and suggest that endochondral ossification was underway (Figure 5d). The junction between the underlying normal bone and the bony outgrowth is richly vascularized by a high concentration of secondary osteons and appears to be marked by a high concentration of osteocyte lacuna (Figure 5d).

4 | DISCUSSION

This study has demonstrated the value of using multiple methods (gross anatomical descriptions, CT scanning and thin sectioning of bones) to assess the nature of the pathologies that afflicted the *Eucyon* specimen (SAM-PQL40041). The same methodologies were also applied to an unafflicted radius to allow us to see how the pathological bone tissue deviated from the unafflicted radius. Our histological observations, that is, the wide OCL present in the peripheral parts of the compacta, permitted us to deduce that the pathological individual was a mature adult that exhibited multiple exostoses on the radius. The worn pattern of the lower dentition preserved corroborated an old age for this individual. The nature of the exostoses has macro- and micro-anatomical characteristics, as well as histological features, which suggest that although these bone tumors were widespread in the skeleton of *E. khoikhoi* (SAM-PQL40041), they were benign, and most likely did not cause any major trauma to the animal. More specifically, except for a couple (e.g., on the humeral proximal epiphysis), most appear to be relatively minor outgrowths that would not have significantly affected the overlying soft tissue, although it is possible that some of the tumors may have impeded efficient locomotion (e.g., those in the phalanges).

4.1 | Anatomical and microanatomical deductions

The gross anatomical observations provided the first indications that several of the bones of the *Eucyon* specimen (SAM-PQL40041) showed an unusual bone surface texture, that suggested a periosteal reactive bone surface (Edeiken et al., 1966). The bone surfaces showed overgrowths of new layers of bone (exostoses) also known as neoplasms or osteomas that extend beyond the surface of the bone (Lewis, 2017; Stilson et al., 2016). As the normal radius (specimen SAM-PQL31272) shows, this is a gross deviation from typical adult bones which have a smooth bone surface. In the study of rhinocerotids, Stilson et al. (2016) ranked the severity of exostoses from 1 to 4: (1) the bone surface is normal; (2) the bone surface shows minor irregular bulging; (3) the bone surface shows protrusions of irregular bone growth; and (4) the bone surface shows the irregular distortion of the non-articular bone surface, with a distortion of the shape of the bone. Considering these categorizations, we would rank the exostoses in our samples as (2)–(3). Even in the most severely affected skeletal element, the exostoses do not deform the original shape of the bone.

Typically, the diagnoses of a bone tumor depend on the following factors: (i) the appearance of the radiograph (i.e., whether the exostosis forms on a peduncle or stalk, like a spur, or whether it is sessile); (ii) the type of periosteal reaction (i.e., is it interrupted or uninterrupted across the bone surface? is their destruction of the underlying bone tissue?) and the location on the bone. There are different types of exostoses: solid with buttresses, solid longitudinal, or solid undulating (Edeiken et al., 1966). Gross inspection of the exostoses evident in our pathological radius revealed that they were solid in texture, and appeared to undulate across the surface of the afflicted bones (Edeiken et al., 1966), and in some areas, they appeared to be thicker than in others. There appears to be an eccentric enlargement of a sessile (as opposed to pedunculated) exostosis on the medial side of the proximal end towards the metaphysis, of the radius. One-sided exostoses are quite commonly observed and have for example been reported in the dinosaur *Edmontosaurus annectens* (BHI 6184) (Anné et al., 2015).

CT scanning of both the normal and pathological bone showed how the pathological radius deviated from what would be the normal condition, and permitted a 3D view of how the entire bone wall was affected. These findings are especially noteworthy, since often in the literature on exostoses, there is a strong focus on the nature of the periosteal reaction, but there is generally no mention of how the underlying endosteal tissues are affected (e.g., Buikstra, 2019). In the CT scan of the afflicted radius, the difference in thickness, and osteoporotic nature of the medial side of the bone wall that underlies the exostosis was evident.

Exostoses have been reported on the patella of the early Cenozoic pantodont, *Coryphodon* (Lucas & Schoch, 1987); and distally in the radius of an Oligocene canid *Hesperocyon* sp., as well as along its shaft (Wang & Rothschild, 1992)—see below. Although x-rays were taken of the bone, the microanatomical details of the radial shaft are not that clear and cannot be compared to the micro-CT scans

that we had taken of the pathological radius of *Eucyon*. Werdelin and Lewis (2013) described a partial skeleton of the jackal *Lupulella* sp., from the Plio-Pleistocene fossil locality of Koobi Fora (Kenya) showing several hyperostosis (e.g., radius, ulna, pisiform and metacarpals). They noted that these pathologies were absent in the metaphyseal region and they lacked areas of sequestration and interpreted them as a systemic infection. Compared at a macroscopic level the pathological individual of *E. khoikhoi* SAM-PQL40041 shows distinct exostoses being more widespread in its skeleton.

4.2 | Deductions based on the histology

The histological thin sections allowed us to examine the microscopic structure of the aberrant bone tissues as compared to the "normal" bone tissues present in the radii of specimens SAM-PQL40041 and SAM-PQL31272, respectively. Besides providing histological details of the exostoses detected macroscopically in SAM-PQL40041, we were able to document for the first time, unusual changes along the endosteal margin of the bone wall. More specifically, our analysis showed that in the case of the large exostosis on the medial side of the bone, columns of calcified cartilage were visible peripherally, particularly near the surface of the exostosis (Figure 5d). Furthermore, within the exostosis, islands of calcified cartilage were evident (Figure 5d). The presence of calcified cartilage overlying the bony growth from the surface of the cortical bone, permits us to diagnose the tumor as an osteochondroma (Dingwall et al., 1970; Pool & Carrig, 1972; Reis et al., 2016). The identification of the exostosis as an osteochondroma was only made possible because the histology of the bone permitted the identification of calcified cartilage along the border of the exostosis. In most cases, exostoses are only identified based on x-rays, and they can appear as simple bony tumors. However, osteochondromas are characterized as being bone tumors that originate on the bone surface to form a projection and are overlain by cartilage (e.g., Lewis, 2017; Reis et al., 2016). The exostoses develop as cartilaginous masses and are progressively replaced by bone through endochondral ossification. Osteochondromas are generally located in long bones, particularly in tubular bones and often at the articular ends or in the metaphyseal regions (e.g., Buikstra, 2019; Dingwall et al., 1970; Pool & Carrig, 1972). In our *Eucyon* specimen, we clearly have an osteochondroma developing further along the diaphysis (away from the metaphasis). It is possible that the condition began when the individual was young, when this region of the bone wall was located more metaphyseally (Enlow, 1962), that is, during post-natal growth the metaphysis becomes incorporated into the diaphysis of long bones. Osteochondromas or osteocartilagenous exostoses are commonly benign bone neoplasms (Buikstra, 2019), and aside from humans, are known to occur in a wide variety of animals, including horses, cats (Pool & Carrig, 1972; Reis et al., 2016), and dogs (Banks & Bridges, 1956; Dingwall et al., 1970). As demonstrated in our pathological radius, benign bone tumors are well differentiated from the bone cortex, and they tend to be slow growing and cause localized effects (e.g., Lewis, 2017).

Wang and Rothschild (1992) reported the presence of osteochondroma in 61% of the museum specimens of the North American Oligocene canid *Hesperocyon* sp., a genus that includes the earliest members of the Family Canidae. Curiously, although the actual size was variable, all affiliated individuals had bony outgrowths on the medial border of the distal radius; and often these were bilaterally symmetrical. Some of the specimens exhibited bony exostoses on the diaphysis as well. In the geologically younger canid we studied, the exostosis occurred on the diaphysis, but prominent sessile exostoses occurred at the proximal ends of several of the bones. Unfortunately, we were not granted permission to thin section these bones, but given their locations, it is quite likely that the latter exostoses represent osteochondromas.

Osteochondromas are generally considered developmental in origin although there are some indications that they may be the result of mutations in the exostosin gene family, or the result of peripheral vascular disease (Buikstra, 2019; Lewis, 2017).

The bony outgrowths are caused by the proliferation and differentiation of chondrocytes that develop away from the growth plate (in the epiphysis). Thus, the cartilage cap over the exostosis undergoes endochondral ossification (as it does at the epiphysis) (Buikstra, 2019). Note that often in dry bones (and fossilized bones) the cartilage cap of the bony tumor is not preserved.

In the pathological *Eucyon* radius we studied, it is very likely that the cartilage layer would have been more substantial, but we are only seeing the calcified cartilage that was preserved during fossilization. This is generally also the case in growing long bones, that is, at the articular ends, only the calcified cartilage is preserved, whereas the overlying disorganized hyaline cartilage is not preserved during the fossilization process (Chinsamy-Turan, 2005). Indeed, if we had not made a thin section in the region of the large exostosis, we would not have been able to identify this exostosis as an osteochondroma. Thus, contrary to the generally held view that such tumors are usually located in the metaphyseal area, we observed this osteochondroma slightly higher up in the diaphysis.

Another aspect of our histological analysis is that we were able to describe the extreme thickening of the endosteal part of the bone wall. These findings contrast with the normal radius wherein both the medial and lateral bone walls were approximately equal in thickness. Additionally, aside from the usual lamellar deposits of the ICL (as in the normal radius), we found that the most recent endosteal deposits in the pathological radius consisted of a more woven type of bone tissue with vascular canals, and globular osteocyte lacunae scattered in the matrix. Furthermore, in some instances, large erosion cavities, reaching cancellous dimensions extended into the medullary cavity. As compared to the "normal" radius, it was also evident that in the pathological radius, there were a lot more erosion cavities in the perimedullary regions. These histological details of the endosteal region of the pathological bone have not been previously reported, probably since most

diagnoses are made from x-rays or CT scan data without any osteohistological assessments.

In other parts of the diaphysis where the exostosis was not as well developed, there appeared to be a thin coating of a narrow layer of bone tissue with more globular osteocyte lacunae that overlies the original periosteal bone margin (Figure 5e). Notably, there appears to be the beginning of another more pronounced exostosis more anteriorly (Figure 5a). Given that there are some unusual secondary osteons near the periosteal margin of both the healthy (Figure 4c) and pathological radius (Figure 5e,g), we propose that these are simply diagenetic and unrelated to the exostoses.

5 | CONCLUSIONS

In this study we were able to apply different methodologies (gross anatomical descriptions, CT scanning, and osteohistology) to identify and diagnose multiple exostoses and an osteochondroma in the skeleton of an early Pliocene canid *E. khoikhoi*. Although several bones in the skeleton showed exostoses, because of the destructive nature of making thin sections, we were only able to section the pathological radius, as well as an unafflicted radius of another specimen of the same species (for comparative purposes), which has limited our understanding of the nature of the other exostoses evident in several bones of SAM-PQL40041.

Our investigation has shown that gross anatomical observations are important for first level identification and characterization of a pathology; after this, micro-CT scanning allows a 3D view of the internal organization of the bony outgrowths. Although most other studies do not undertake osteohistological analyses, we propose that even though such analyses are destructive, if possible, histological sections should be prepared of the pathology, since they provide unparalleled information regarding the nature of the tissues associated with the pathology. In our study, although the anatomical descriptions and CT scanning allowed us to recognize the exostoses as benign bone tumors, if we had not prepared thin sections of the bone, we would not have been able to identify the medial exostosis on the radius as an osteochondroma, and we would not have been able to describe the associated deviant endosteally formed bone tissues. Given the predominance of exostosis in the articular ends of the bones of this individual, it is likely that the pathology was systemic, and we propose that these exostoses are likely to also be osteochondromas. Unfortunately, such diagnoses will need thin sectioning of the bones, and it is unlikely that permission would be granted to do this. However, we propose that at the very least CT scan studies could be conducted to investigate the pathologies evident on the mandibles of *E. khoikhoi*, since these appear to be starkly different from the exostoses observed elsewhere in the skeleton.

AUTHOR CONTRIBUTIONS

A.C. and A.V. conceived and designed the study. Both authors contributed to data collection, figure development and analyses. All authors edited, reviewed, and approved the submitted manuscript.

ACKNOWLEDGEMENTS

We thank the curator Dr. Romala Govender (Iziko Museums of South Africa) and the collection manager Sarena Govender (Iziko Museums of South Africa) for access to the material under their care. We express our gratitude to Ragna Redelstorff (South African Heritage Resources Agency) for permission to conduct the destructive analysis. We are also grateful to Carmen Nacarino Meneses (Institut Català de Paleontologia Miquel Crusafont) for assistance with the preparation of the histological samples in 2020, and Sian Wood for final preparation of the thin sections. Maria-Eugenia Pereyra is thanked for providing useful comments on an earlier draft of the MS. AV is also grateful for support from the Research Group UCM 910607, the project PID2020-116220GB-I00 (Ministerio de Investigación e Innovación), and Project PID2023-151089NB-I00 funded by MCIU/AEI /10.13039/501100011033/FEDER, UE. AC was supported by the National Research Foundation, South Africa, grant number, 136510. We thank the Editor Mateusz Wosik, and two anonymous reviewers for their useful comments and suggestions, which have improved our manuscript.

CONFLICT OF INTEREST STATEMENT

The authors declare that they have no competing interests.

DATA AVAILABILITY STATEMENT

Higher resolution images that support the findings of this study are available on request from the corresponding author.

ORCID

Anusuya Chinsamy https://orcid.org/0000-0002-9786-5080
Alberto Valenciano https://orcid.org/0000-0003-1633-2248

REFERENCES

Anné, J., Garwood, R.J., Lowe, T., Withers, P.J. & Manning, P.L. (2015) Interpreting pathologies in extant and extinct archosaurs using micro-CT. *PeerJ*, 3, e1130. Available from: https://doi.org/10.7717/peerj.1130

Banks, W. & Bridges, C. (1956) Multiple cartilaginous exostoses in a dog. *Journal of the American Veterinary Medical Association*, 129, 131–135.

Bartolini-Lucenti, S., Madurell-Malapeira, J., Martínez-Navarro, B., Palmqvist, P., Lordkipanidze, D. & Rook, L. (2021) The early hunting dog from Dmanisi with comments on the social behaviour in Canidae and hominins. *Scientific Reports*, 11, 13501. Available from: https://doi.org/10.1038/s41598-021-92818-4

Bernor, R.L. & Kaiser, T.M. (2006) Systematics and paleoecology of the earliest Pliocene equid, *Eurygnathohippus hooijeri* n. sp. from Langebaanweg, South Africa. *Mitteilungen aus dem Hamburgischen zoologischen Museum und Institut*, 103, 149–186.

Buikstra, J.E. (2019) *Ortner's identification of pathological conditions in human skeletal remains*. London: Academic Press.

Calderón, T., Arnold, W., Stalder, G., Painer, J. & Köhler, M. (2021) Labelling experiments in red deer provide a general model for early bone growth dynamics in ruminants. *Scientific Reports*, 11, 14074. Available from: https://doi.org/10.1038/s41598-021-93547-4

Chinsamy, A. & Raath, M.A. (1992) Preparation of fossil bone for histological study. *Palaeontologia Africana*, 29, 39–44.

Chinsamy, A. & Tumarkin-Deratzian, A. (2009) Pathologic bone tissues in a Turkey vulture and a nonavian dinosaur: implications for interpreting endosteal bone and radial fibrolamellar bone in fossil dinosaurs. *The Anatomical Record*, 292, 1478–1484. Available from: https://doi.org/10.1002/ar.20991

Chinsamy, A. & Warburton, N.M. (2021) Ontogenetic growth and the development of a unique fibrocartilage entheses in *Macropus fuliginosus*. *Zoology*, 144, 125860. Available from: https://doi.org/10.1016/j.zool.2020.125860

Chinsamy-Turan, A. (2005) *The microstructure of dinosaur bone: deciphering biology with fine scale techniques*. Baltimore: Johns Hopkins University Press.

de Souza Barbosa, F.H., de Oliveira Porpino, K. & Fragoso, A.B.L. (2013) Osteomyelitis in Quaternary mammal from the Rio Grande do Norte State, Brazil. *Quaternary International*, 299, 90–93. Available from: https://doi.org/10.1016/j.quaint.2012.12.035

Dingwall, J., Pass, D., Pennock, P. & Cawley, A. (1970) Case report. Multiple cartilaginous exostoses in a dog. *The Canadian Veterinary Journal*, 11, 114.

Domingo, M.S., Alberdi, M.T., Azanza, B. & Morales, J. (2012) Mortality patterns and skeletal physical condition of the carnivorans from the Miocene assemblage of Batallones-1 (Madrid Basin, Spain). *Neues Jahrbuch fur Geologie und Palaontologie-Abhandlungen*, 265, 131–145. Available from: https://doi.org/10.1127/0077-7749/2012/0251

du Plessis, A., Broeckhoven, C., Guelpa, A. & Le Roux, S.G. (2017) Laboratory X-ray microcomputed tomography: a user guideline for biological samples. *GigaScience*, 6, 1–11. Available from: https://doi.org/10.1093/gigascience/gix027

du Plessis, A., Le Roux, S.G. & Guelpa, A. (2016) The CT scanner facility at Stellenbosch University: an open access X-ray computed tomography laboratory. *Nuclear Instruments and Methods in Physics Research Section B: Beam Interaction with Materials and Atoms*, 384, 42–49. Available from: https://doi.org/10.1016/j.nimb.2016.08.005

Edeiken, J., Hodes, P.J. & Caplan, L.H. (1966) New bone production and periosteal reaction. *American Journal of Roentgenology*, 97, 708–718.

Ekhtiari, S., Chiba, K., Popovic, S., Crowther, R., Wohl, G., Wong, A.K.O. et al. (2020) First case of osteosarcoma in a dinosaur: a multimodal diagnosis. *The Lancet Oncology*, 21, 1021–1022. Available from: https://doi.org/10.1016/S1470-2045(20)30171-6

Enlow, D.H. (1962) A study of the post-natal growth and remodelling of bone. *American Journal of Anatomy*, 110, 79–102.

Fernández-Monescillo, M., Antoine, P.-O., Quispe, B.M., Münch, P., Flores, R.A., Marivaux, L. et al. (2019) Multiple skeletal and dental pathologies in a late Miocene mesotheriid (Mammalia, Notoungulata) from the Altiplano of Bolivia: palaeoecological inferences. *Palaeogeography, Palaeoclimatology, Palaeoecology*, 534, 109297. Available from: https://doi.org/10.1016/j.palaeo.2019.109297

Franz-Odendaal, T.A., Chinsamy, A. & Lee-Thoro, J.A. (2004) High prevalence of enamel hypoplasia in an early Pliocene giraffid (*Sivatherium hendeyi*) from South Africa. *Journal of Vertebrate Paleontology*, 24, 235–244. Available from: https://doi.org/10.1671/19

Gentry, A.W. (1980) Fossil Bovidae (Mammalia) from Langebaanweg South Africa. *Annals of the South African Museum*, 79, 213–337.

González, R., Gallina, P.A. & Cerda, I.A. (2017) Multiple paleopathologies in the dinosaur *Bonitasaura salgadoi* (Sauropoda: Titanosauria) from the Upper Cretaceous of Patagonia, Argentina. *Cretaceous Research*, 79, 159–170. Available from: https://doi.org/10.1016/j.cretres.2017.07.013

Govender, R. (2015) Preliminary phylogenetics and biogeographic history of the Pliocene seal, *Homiphoca capensis* from Langebaanweg, South Africa. *Transactions of the Royal Society of South Africa*, 70, 25–39. Available from: https://doi.org/10.1080/0035919X.2014.984258

Govender, R., Avery, G. & Chinsamy, A. (2011) Pathologies in the Early Pliocene phocid seals from Langebaanweg, South Africa. *South African Journal of Science*, 107, 72–77. Available from: https://doi.org/10.4102/sajs.v107i1/2.230

Govender, R., Chinsamy, A. & Ackerman, R.R. (2012) Anatomical and landmark morphometric analysis of fossil phocid seal remains from Langebaanweg, West Coast of South Africa. *Transactions of the Royal Society of South Africa*, 67, 135–149. Available from: https://doi.org/10.1080/0035919X.2012.724471

Haridy, Y., Witzmann, F., Asbach, P., Schoch, R.R., Frobisch, N. & Rothschild, B.M. (2019) Triassic cancer-osteosarcoma in a 240-million-year-old stem-turtle. *JAMA Oncology*, 5, 425–426. Available from: https://doi.org/10.1001/jamaoncol.2018.6766

Harris, J.M. (1976) Pliocene Giraffoidea (Mammalia, Artiodactyla) from the Cape Province. *Annals of the South African Museum*, 69, 325–353.

Heckert, A.B., Viner, T.C. & Carrano, M.T. (2021) A large, pathological skeleton of *Smilosuchus gregorii* (Archosauriformes: Phytosauria) from the Upper Triassic of Arizona, USA, with discussion of the paleobiological implications of paleopathology in fossil archosauromorphs. *Palaeontologia Electronica*, 24, 1–36. Available from: https://doi.org/10.26879/1123

Hendey, Q.B. (1970) The age of the fossiliferous deposits at Langebaanweg, Cape Province, South African Museum. *Annals of the South African Museum*, 56, 119–131.

Hendey, Q.B. (1973) Fossil occurrences at Langebaanweg, Cape Province. *Nature*, 244, 13–14.

Hendey, Q.B. (1974) The Late Cenozoic Carnivora of the South-Western Cape Province. *Annals of the South African Museum*, 63, 1–369.

Hendey, Q.B. (1978a) Late Tertiary Hyaenidae from Langebaanweg, South Africa, and their relevance to the phylogeny of the family. *Annals of the South African Museum*, 76, 265–297.

Hendey, Q.B. (1978b) Late Tertiary Mustelidae (Mammalia, Carnivora) from Langebaanweg, South Africa. *Annals of the South African Museum*, 76, 329–357.

Hendey, Q.B. (1980) *Agriotherium* (Mammalia, Ursidae) from Langebaanweg, South Africa, and the relationships of the genus. *Annals of the South African Museum*, 81, 1–110.

Hendey, Q.B. (1981) Palaeoecology of the late Tertiary fossil occurrences in 'E' Quarry, Langebaanweg, South Africa, and a reinterpretation of their geological context. *Annals of the South African Museum*, 84, 1–104.

Hendey, Q.B. (1982) *Langebaanweg: a record of the past*. Wynberg: Rustica Press.

Hendey, Q.B. & Gentry, A.W. (1970) A Review of the Geology and Palaeontology of the Plio, Pleistocene Deposits at Langebaanweg, Cape Province. *Annals of the South African Museum*, 56, 75–117.

Hill, R.V. (2006) Comparative anatomy and histology of xenarthran osteoderms. *Journal of Morphology*, 267, 1441–1460. Available from: https://doi.org/10.1002/jmor.10490

Hunt, R., Jr. (1996) Basicranial anatomy of the giant viverrid from 'E' Quarry, Langebaanweg, South Africa. In: Stewart, K.M. & Seymour, K.L. (Eds.) *Palaeoecology and palaeoenvironments of Late Cenozoic mammals: tributes to the career of CS (Rufus) Churcher*. Toronto: University of Toronto Press, pp. 588–597. Available from: https://doi.org/10.3138/9781487574154

Iurino, D.A., Fico, R., Petrucci, M. & Sardella, R. (2013) A pathological Late Pleistocene canid from San Sidero (Italy): implications for social- and feeding-behaviour. *Naturwissenschaften*, 100, 235–243. Available from: https://doi.org/10.1007/s00114-013-1018-5

Iurino, D.A., Fico, R. & Sardella, R. (2015) A pathological Late Pleistocene badger from San Sidero (Apulia, Southern Italy): implications for developmental pathology and feeding behaviour. *Quaternary International*, 366, 96–101. Available from: https://doi.org/10.1016/j.quaint.2014.12.030

Iurino, D.A. & Sardella, R. (2015) Medical CT scanning and the study of hidden oral pathologies in fossil carnivores. *Paläontologische Zeitschrift*, 89, 251–259. Available from: https://doi.org/10.1007/s12542-013-0220-2

Jannello, J. & Chinsamy, A. (2023) Osteohistology and palaeobiology of giraffids from the Mio-Pliocene Langebaanweg (South Africa). *Journal of Anatomy*, 242, 953–971. Available from: https://doi.org/10.1111/joa.13825

Jiangzuo, Q., Rabe, C., Abella, J., Govender, R. & Valenciano, A. (2023) Langebaanweg's sabertooth guild reveals an African Pliocene evolutionary hotspot for sabertooths (Carnivora; Felidae). *Iscience*, 26, 107212. Available from: https://doi.org/10.1016/j.isci.2023.107212

Kohler, M. & Moya-Sola, S. (2009) Physiological and life history strategies of a fossil large mammal in a resource-limited environment. *Proceedings of the National Academy of Sciences*, 106, 20354–20358. Available from: https://doi.org/10.1073/pnas.0813385106

Kolb, C., Scheyer, T.M., Veitschegger, K., Forasiepi, A.M., Amson, E., van der Geer, A.A. et al. (2015) Mammalian bone palaeohistology: a survey and new data with emphasis on Island forms. *PeerJ*, 3, e1358. Available from: https://doi.org/10.7717/peerj.1358

Legendre, L.J. & Botha-Brink, J. (2018) Digging the compromise: investigating the link between limb bone histology and fossoriality in the aardvark (*Orycteropus afer*). *PeerJ*, 6, e5216. Available from: https://doi.org/10.7717/peerj.5216

Lewis, M. (2017) *Paleopathology of children: identification of pathological conditions in the human skeletal remains of non-adults*. London: Academic Press.

Lucas, S.G. & Schoch, R.M. (1987) Paleopathology of Early Cenozoic *Coryphodon* (Mammalia; Pantodonta). *Journal of Vertebrate Paleontology*, 7, 145–154. Available from: https://doi.org/10.1080/02724634.1987.10011649

Luna, C.A., Pool, R.R., Ercoli, M.D., Chimento, N.R., Barbosa, F.H.D.S., Zurita, A.E. et al. (2023) Osteomyelitis in the manus of *Smilodon populator* (Felidae, Machairodontinae) from the Late Pleistocene of South America. *Palaeoworld*, 33, 517–525. Available from: https://doi.org/10.1016/j.palwor.2023.05.001

Matthews, T., Denys, C. & Parkington, J.E. (2007) Community evolution of Neogene micromammals from Langebaanweg 'E' Quarry and other west coast fossil sites, south-western Cape, South Africa. *Palaeogeography, Palaeoclimatology, Palaeoecology*, 245, 332–352. Available from: https://doi.org/10.1016/j.palaeo.2006.08.015

Moncunill-Solé, B., Isidro, A., Blanco, A., Angelone, C., Rössner, G.E. & Jordana, X. (2019) The most ancient evidence of a diseased lagomorph: infectious paleopathology in a tibiofibular bone (Middle Miocene, Germany). *Comptes Rendus Palevol*, 18, 1011–1023. Available from: https://doi.org/10.1016/j.crpv.2019.10.007

Montoya-Sanhueza, G., Bennett, N.C., Oosthuizen, M.K., Dengler-Crish, C.M. & Chinsamy, A. (2021) Bone remodeling in the longest living rodent, the naked mole-rat: interelement variation and the effects of reproduction. *Journal of Anatomy*, 239, 81–100. Available from: https://doi.org/10.1111/joa.13404

Montoya-Sanhueza, G. & Chinsamy, A. (2018) Cortical bone adaptation and mineral mobilization in the subterranean mammal *Bathyergus suillus* (Rodentia: Bathyergidae): effects of age and sex. *PeerJ*, 6, e4944. Available from: https://doi.org/10.7717/peerj.4944

Moodie, R.L. (1923) *Palaeopathology*. Urbana: University of Illinois Press.

Nacarino-Meneses, C. & Chinsamy, A. (2022) Mineralized-tissue histology reveals protracted life history in the Pliocene three-toed horse from Langebaanweg (South Africa). *Zoological Journal of the Linnean Society*, 196, 1117–1137. Available from: https://doi.org/10.1093/zoolinnean/zlab037

Nacarino-Meneses, C., Jordana, X. & Köhler, M. (2016) First approach to bone histology and skeletochronology of *Equus hemionus*. *Comptes Rendus Palevol*, 15, 267–277. Available from: https://doi.org/10.1016/j.crpv.2015.02.005

Pool, R. & Carrig, C. (1972) Multiple cartilaginous exostoses in a cat. *Veterinary Pathology*, 9, 350–359. Available from: https://doi.org/10.1177/030098587200900505

Rabe, C., Chinsamy, A. & Valenciano, A. (2022) Taxonomic and palaeobiological implications of a large, pathological sabretooth (Carnivora, Felidae, Machairodontinae) from the Lower Pliocene of South Africa. *Papers in Palaeontology*, 8, e1463. Available from: https://doi.org/10.1002/spp2.1463

Redelstorff, R., Hayashi, S., Rothschild, B.M. & Chinsamy, A. (2015) Non-traumatic bone infection in stegosaurs from Como Bluff, Wyoming. *Lethaia*, 48, 47–55. Available from: https://doi.org/10.1111/let.12086

Reis, M.D.O., Mello, L.S.D., Hesse, K.L., Lorenzett, M.P., Reis, K.D.H.L.D., Campos, F.S. et al. (2016) Osteochondroma in a young cat infected by feline leukemia virus. *Ciência Rural*, 47, 1–4. Available from: https://doi.org/10.1590/0103-8478cr20151558

Roberts, D.L., MatthewS, T., Herries, A.I.R., Boulter, C., Scott, L., Dondo, C. et al. (2011) Regional and global context of the Late Cenozoic Langebaanweg (LBW) palaeontological site: West Coast of South Africa. *Earth-Science Reviews*, 106, 191–214. Available from: https://doi.org/10.1016/j.earscirev.2011.02.002

Rothschild, B.M., Rothschild, C. & Woods, R.J. (2001) Inflammatory arthritis in canids: spondyloarthropathy. *Journal of Zoo and Wildlife Medicine*, 32, 58–64. Available from: https://doi.org/10.1638/1042-7260(2001)032[0058:IAICS]2.0.CO;2

Seymour, K., Reynolds, A. & Churcher, C. (2018) Smilodon fatalis from Talara, Peru: sex, age, mass, and histology. In: Werdelin, L., Mcdonald, H. & Shaw, C. (Eds.) *Smilodon: the iconic sabertooth*. Baltimore, MD: Johns Hopkins University Press, pp. 30–52.

Slabá, K., Kryštufek, B. & Nemec, A. (2018) Oral and dental examination findings in Beech Martens (*Martes foina*). *Journal of Comparative Pathology*, 163, 10–17. Available from: https://doi.org/10.1016/j.jcpa.2018.06.004

Stilson, K.T., Hopkins, S.S. & Davis, E.B. (2016) Osteopathology in Rhinocerotidae from 50 million years to the present. *PLoS One*, 11, e0146221. Available from: https://doi.org/10.1371/journal.pone.0146221

Tong, H., Chen, X., Zhang, B., Rothschild, B., White, S., Balisi, M. et al. (2020) Hypercarnivorous teeth and healed injuries to *Canis chihliensis* from Early Pleistocene Nihewan beds, China, support social hunting for ancestral wolves. *PeerJ*, 8, e9858. Available from: https://doi.org/10.7717/peerj.9858

Valenciano, A. & Govender, R. (2020a) New fossils of *Mellivora benfieldi* (Mammalia, Carnivora, Mustelidae) from Langebaanweg, 'E' Quarry (South Africa, Early Pliocene): re-evaluation of the African Neogene mellivorines. *Journal of Vertebrate Paleontology*, 40, e1817754. Available from: https://doi.org/10.1080/02724634.2020.1817754

Valenciano, A. & Govender, R. (2020b) New insights into the giant mustelids (Mammalia, Carnivora, Mustelidae) from Langebaanweg fossil site (West Coast Fossil Park, South Africa, early Pliocene). *PeerJ*, 8, e9221. Available from: https://doi.org/10.7717/peerj.9221

Valenciano, A., Morales, J. & Govender, R. (2022) *Eucyon khoikhoi* sp. nov. (Carnivora: Canidae) from Langebaanweg 'E' Quarry (early Pliocene, South Africa): the most complete African canini from the Mio-Pliocene. *Zoological Journal of the Linnean Society*, 194, 366–394. Available from: https://doi.org/10.1093/zoolinnean/zlab022

Wang, D., Xing, L., Rothschild, B.M., Persons, W.S., IV & Liu, J. (2023) A palaeopathological specimen of the Late Miocene *Parataxidea* sp.(Mammalia: carnivora) from the Linxia Basin, China. *Historical Biology*, 35, 1255–1260. Available from: https://doi.org/10.1080/08912963.2022.2086802

Wang, X. & Rothschild, B.M. (1992) Multiple hereditary osteochondroma in oligocene *Hesperocyon* (Carnivora: Canidae). *Journal of Vertebrate Paleontology*, 12, 387–394.

Werdelin, L. (2006) The position of Langebaanweg in the evolution of Carnivora in Africa. *African Natural History*, 2, 201–202.

Werdelin, L. & Lewis, M.E. (2013) *Koobi fora research project volume 7: the carnivora*. San Francisco: California Academy of Sciences.

Werdelin, L., Turner, A. & Solounias, N. (1994) Studies of fossil hyaenids: the genera *Hyaenictis Gaudry* and *Chasmaporthetes Hay*, with a re-consideration of the Hyaenidae of Langebaanweg, South Africa. *Zoological Journal of the Linnean Society*, 111, 197–217. Available from: https://doi.org/10.1006/zjls.1994.1022

Woolley, M.R., Chinsamy, A., Govender, R. & Bester, M.N. (2019) Microanatomy and histology of bone pathologies of extant and extinct phocid seals. *Historical Biology*, 33, 1231–1246. Available from: https://doi.org/10.1080/08912963.2019.1689238

How to cite this article: Chinsamy, A. & Valenciano, A. (2025) Multiple exostoses and an osteochondroma in a Pliocene canid from Langebaanweg 'E' Quarry (South Africa). *Journal of Anatomy*, 247, 856–868. Available from: https://doi.org/10.1111/joa.14133